EAM
Environmental and Materials
EAM 1(2): 74–86
ISSN 3025-0277

Electroreduction of carbon dioxide (CO_2) with flow cell system using tin-modified copper foam electrode

Muhammad Iqbal Syauqi [1*], Annisa Titi Cahyani [1], Yulia Mariana Tesa Ayudia Putri [1], and Prastika Krisma Jiwanti [2]

[1] Department of Chemistry, Faculty of Mathematics and Natural Sciences, Universitas Indonesia; 16424 Depok, West Java, Indonesia
[2] Nanotechnology Engineering, Faculty of Advanced Technology and Multidiscipline, Universitas Airlangga; Surabaya 60115, Indonesia
* Correspondence: muhammad.iqbal@sci.ui.ac.id

Accepted Date: December 31, 2023

Cite This Article:
Syauqi, M. I., Cahyani, A. T., Putri, Y. M. T. A., & Jiwanti, P. K. (2023). Electroreduction of carbon dioxide (CO2) with flow cell system using tin-modified copper foam electrode. *Environmental and Materials, 1*(2), 74-86. https://doi.org/10.61511/eam.v1i2.2023.363

Abstract
In this study, modification of the copper foam (Cuf) electrode with tin (Sn) was carried out with the electrodeposition method for application in CO_2 electroreduction. Characterization using SEM EDX, FTIR, and XRD confirmed the presence of Cu_2O, CuO, and SnO_2 thin layer mixture on the Cuf/Sn electrode. The electrochemical characteristics of the electrode were examined by using the cyclic voltammetry (CV) technique. Under optimized conditions, electrochemical reduction of CO_2 in a flow cell system. At the optimum condition of CO_2 reduction in a flow cell system (flow rate of 75 mL/min and −0.6 V vs Ag/AgCl applied potential), the Cuf/Sn electrode exhibited a remarkable 75.79% with an 8.84 µmol/h formic acid production rate. In a comparable experiment, the Cuf/Sn flow system revealed a twofold improvement in the faradaic efficiency compared to the batch system and a threefold increase compared to the unmodified Cuf electrode in the flow system. Stability tests demonstrated consistent performance up to the 4th cycle, followed by a decline in the 5th cycle, potentially indicative of surface deterioration. The elevated performance is attributed to the synergistic effect of the Cu-Sn oxide layer, reinforcing the catalyst's potential for efficient electrochemical CO_2 reduction to formic acid.
Keywords: carbon dioxide; copper foam; electroreduction; flow system; formic acid; tin

1. Introduction

The rising concentration of carbon dioxide (CO_2) in the Earth's atmosphere, primarily attributed to anthropogenic activities such as industrial processes, fossil fuel combustion, and deforestation, has led to significant environmental concerns (Canadell et al., 2007; Song, 2002). This surge in CO_2 levels contributes to the greenhouse effect, leading to global warming, ecological disruptions, and adverse effects on human health (Florides & Christodoulides, 2009). To mitigate these adverse effects, it is necessary to devise strategies for converting CO_2 into another chemical that is more valuable or at least less harmful.

Various methods and technologies, including thermal, photochemical, and electrochemical approaches have been reported used for CO_2 conversion by using reduction reaction pathways (Jiwanti et al., 2020; Kondratenko et al., 2013; Yang et al., 2020). Among these methods, electrochemical reduction stands out as a promising technique in CO_2 reduction due to its simple operation, high efficiency, and potential opportunities for large-scale applications (Sun et al., 2017). Moreover, the electrochemical conversion of CO_2 can be carried out at atmospheric pressure and temperature to produce fuels and valuable chemicals, making it ideal for large-scale implementation and integration (Feaster et al., 2017). However, one of the major bottlenecks of CO_2 electrochemical reduction is the diverse products that might be produced, ranging from carbon monoxide, carboxylic acid, aldehyde, alcohol, and hydrocarbons. Therefore, there is a need to devise a method that

enhances selectivity towards certain products of the electrochemical system, to make it suitable for industrial practice. Among all approaches, constructing a unique electrocatalyst is believed to be the main prospect to achieve acceptable system selectivity.

Amidst the diverse array of possible products of CO_2 reduction, formic acid has gained significant attention. This interest is caused by the high utility of formic acid in industrial applications including preservatives, coagulants, and potential fuel. The high energy density of formic acid along with its liquid form at room temperature, makes it suitable for energy storage and transport application. Furthermore, the conversion of CO_2 to formic acid is kinetically preferred as it only requires 2 electrons and protons transfer.

Copper (Cu) has emerged as one of the most studied electrocatalysts for the conversion of CO2 into renewable fuels such as hydrocarbons and alcohols due to its low cost and unique interaction with CO_2 (De Gregorio et al., 2020; Gonçalves et al., 2013). Reports in the literature state that various forms of copper structures, particularly in a nanoporous foam, exhibit success in converting CO_2 into diverse products such as CO, methane, formic acid, ethanol, ethylene, and higher hydrocarbons (Sen et al., 2014; Zeng et al., 2018). This new electrode has a larger and specific surface area that can provide a more active site for accelerating electrochemical reactions. However, Cu-based electrodes often exhibit low selectivity for formic acid production in aqueous electrolytes. It has been reported that CO_2 electroreduction on copper foam with hierarchical porosity resulted in the highest Faradaic efficiency for formic acid production of 29% (Sen et al., 2014). One strategy to overcome this challenge involves combining Cu with another metal to create a unique surface condition favoring a selective two-electron and proton transfer to CO_2, leading to the formation of formic acid (Saprudin et al., 2023). Previous studies have demonstrated successful outcomes by coupling Cu with Ni (Jiwanti et al., 2019) or Cu with Au (Saprudin et al., 2023), despite a still unsatisfactory faradaic efficiency (below 50%). Conversely, Tin (Sn) metal or its oxide form (SnO_2) has emerged as a catalyst that can selectively reduce CO_2 to formic ion (HCOO-) with faradaic efficiency > 70% (Li et al., 2020; Liu et al., 2018; Proietto et al., 2023). Moreover, Sn-based catalyst holds promise for large-scale application considering the relatively high abundance of Sn in the earth's crust and its good chemical stability (Feaster et al., 2017). Thus, combining the unique Cu and Sn interaction may be the key to achieving the high selectivity of formic acid production from CO_2.

Tin-modified copper foam (Sn/f-Cu) electrodes has been introduced by Wang et al In 2016, demonstrating significant advancements in formic acid production with a Faradaic efficiency reaching 83.5% in a static (batch) system. Another work from Fan et al reported the use of CuO–SnO_2 electrode achieving a 74.4% faradaic efficiency (Fan et al., 2018) also in a batch system. Nevertheless, the application of static cells imposes limitations on current densities (<100 mA/cm2) due to mass transport constraints (Weekes et al., 2018).

In the present study, we aim to extend these findings by investigating CO_2 electroreduction using Sn-modified Cu foam (Cuf/Sn) electrodes with a flow cell system. Different from the other, the modification was conducted by using anodic electrodeposition in a citrate complex leading to a unique mixture of Cu-Sn oxide thin layer on Cuf. The use of a flow reactor provides more control over reagent delivery. This configuration is expected to mitigate the mass transport challenges encountered in batch systems, which can potentially lead to a higher current density (J) and improved electrochemical performance (Zahran Ilyasa et al., 2020).

2. Methods

2.1. Chemicals

Copper foam (Cu foam 98.99%, 1 mm thick) was purchased from Futiantian Technology Co., Ltd. Tin (II) chloride dihydrate ($SnCl_2.2HO_2$, 99.9%), sodium citrate dihydrate ($Na_3C6H_5O_7$), ethanol absolute (C_2H_5OH), sulfuric acid (H_2SO_4, 98%), potassium bicarbonate ($KHCO_3$, 99.7%), perchloric acid ($HClO_4$, 99%), potassium hydroxide (KOH, 99.99%) and methanol for liquid chromatography (CH_3OH), all reagents purchased from Merck were used without

further purification. Ultrapure water was obtained using the Symply-Lab water purification system (Direct-Q 5 UV, Millipore).

2.2. Synthesis of Cuf/Sn Electrode

The synthesis of the Cuf/Sn electrode refers to the experiment that has been carried out by Wang, et al. (Wang et al., 2016) in 2016 with modification. Cuf with 1 mm thickness was sonicated in isopropanol and deionized water to remove impurities and dried at room temperature before being used as a substrate for electrochemical deposition. The electrolyte used was made by dissolving sodium citrate in deionized water to form a 0.05 M solution, then the pH was adjusted to 6 by adding 0.1 M H_2SO_4. Then $SnCl_2$ was added into the solution to make 0.018 M Sn^{2+}. The solution was moderately stirred for 10 h before the electrodeposition process commencement. The Sn-based film was deposited on the Cu substrate by galvanostatic electroplating at +4.8 mA for 30 minutes. The final deposits were sequentially rinsed with methanol and deionized water, and the sample obtained was marked as Cuf/Sn after dried in open air.

2.3. Materials Characterization

The morphology and structure of Cu and Cuf/Sn electrodes were characterized by scanning electron microscopy (SEM) and energy dispersion spectroscopy (EDS) was obtained on a Hitachi S-4800 at an acceleration voltage of 15 kV. The surface chemistry properties of the electrodes were analyzed with Fourier transform infrared spectroscopy (FTIR) Alpha Bruker. X-ray diffraction pattern (XRD) was recorded on a Bruker D8 Focus diffractometer using Cu Kα radiation (λ=1.54056 Å), scan range from 20 to 80o.

2.4. Electrochemical Measurements

The electrochemical experiments were performed in a typical H-type electrolytic cell separated by a proton exchange membrane (Nafion 117) using potentiostat Autolab PGStat 204. Ag/AgCl electrode (sat. KCl) was applied as the reference electrode and a Pt spiral was chosen as the counter electrode. The Cuf and Cuf/Sn with a geometric surface area of 1 cm^2 were used as the working electrode. An aqueous solution of 0.,1 M $KHCO_3$ was prepared as the electrolyte. Before the electroreduction process, N_2 and CO_2 were continuously blown into electrolyte at 15 minutes for N_2 and then 30 minutes for CO_2 with a constant rate (100 mL min-1) to form CO_2-saturated 0.1 M $KHCO_3$ (pH=7.2) solution. Cyclic voltammetry (CV) experiments were performed in a three-electrode cell. The electrolyte was a N_2 or CO_2 saturated 0.1 M $KHCO_3$ aqueous solution. CV was performed from –0.8 V to 0.4 V at a scan rate of 50 mV/s.

The electrochemical surface area (EASA) test using 1mM $K_3Fe(CN)_6$ was diluted in 0.1 M phosphate-buffered saline pH 7 as electrolyte. All experiments were performed at room temperature (20–30 ^oC) and ambient pressure.

2.5. CO_2 Reduction Experiments

The CRR experiments were conducted in a custom-made two-compartment cell with a proton exchange membrane (Nafion 117) as the separator. The volume of the electrolyte was approximately 15 mL in each of the two compartments. The chronoamperometric measurements (CA) for 1 hour were carried out by using a potentiostat with Cuf or Cuf/Sn as the working electrode, Ag/AgCl as a reference, and Pt spiral as the counter electrode. The CRR in the flow cell system was carried out under variations of flow rate (65, 75, and 100 mL/min) and reduction potential (–0.3, –0.5, –0.6 V vs Ag/AgCl). The flow system performance was also compared with the batch system. The formic acid produced from the CO_2 electroreduction process was taken from the catholyte and then analyzed using high-performance liquid chromatography (HPLC) using. Inertsil ODS-3.5 µm GL Science Inc. column (40^oC) with 0.1 % $HClO_4$ as mobile phase (1mL/min flow rate), and 30 µL sample injection volume. This method gives formic acid retention time of ~2.35 min. To calculate the formic acid generated from the reaction, sample's peak area was compared with the standards. Calibration curve with formula y = 106.25x + 427.52 and r2 = 0.9994 was

obtained by plotting peak area against the concentration of formic acid standard solutions (0 – 500 ppm). Afterwards, the corresponding Faradaic efficiency were calculated based on the following equation:

$$\text{Faradaic efficiency (FE)} = \frac{\text{mol formic acid generated}}{\text{Q / F x n}} \qquad (1)$$

Where F is the Faraday constant (96485), n is the number of electrons used for producing one molecule liquid product (in the case of formic acid, n = 2) and Q is the total quantity of electric charge (A s)

3. Results and Discussion

3.1. Synthesis and Characterization of Cuf and Cuf/Sn Electrode

In the synthesis of the Cuf/Sn electrode, the Sn electrodeposition was performed at the anode in the presence of sodium citrate ($Na_3C_6H_5O_7$) as a complex agent to maintain the stability of tin layer formation on the surface of the Cuf (El Bahi et al., 2020). In pH 6, the complex can be present in the form of $Sn[C_6H_5O_7]^{2-}$ or $SnH_2C_6H_5O_7$, which have a higher activation energy than Sn^{2+} so that the deposition will occur slowly and more controllable (Slupska & Ozga, 2014). The modification of Cuf with this technique was expected to give a small amount of oxide on the surface of Cuf. Figure 1a gives the SEM morphology of Cuf, showing a microporous foam-like structure. The EDS result of Cuf in Figure 1b shows that the surface of Cuf has been cleaned as it shows ~100% Cu response with a negligible amount of oxygen peak. The electrodeposition of Cuf made the color of Cuf to become darker as shown in Figure 1c. Furthermore, it can be seen from Figure 1d that the surface of the Cuf/Sn electrode has been covered by a homogenous granular particle. The EDS spectrum of Cuf/Sn in Figure 1e confirms the presence of small Sn and O peaks owing to a 0.22% and 0.50% weight for Sn and O, respectively. The atomic % of O reached 1.94%, while the Sn %atomic that only 0.12% indicating that the surface of Cuf has been modified by not only Sn oxide but also the oxides of Cu. Cross section SEM image in Figure 1f estimates the average thickness of the oxides layer was 1.65 µm.

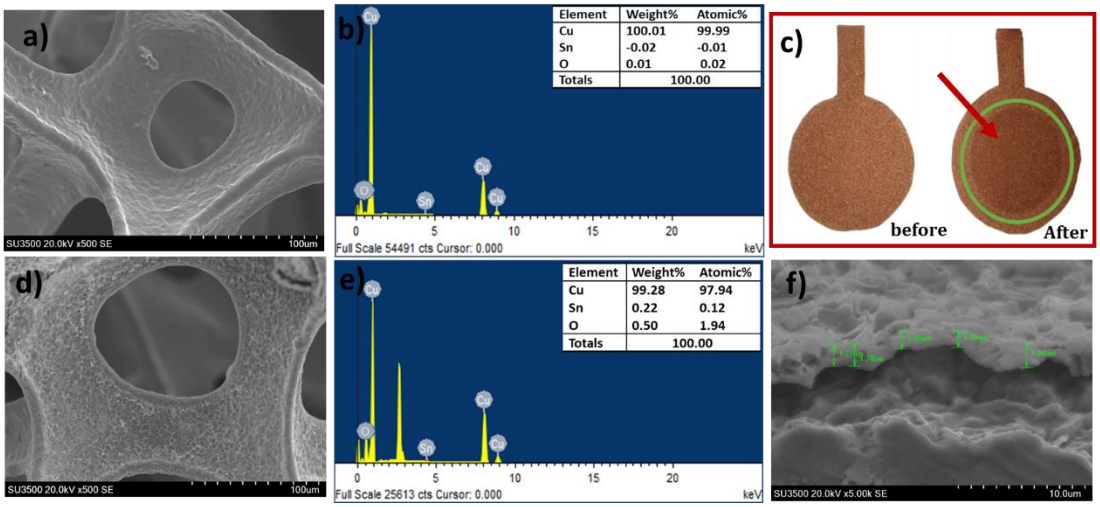

Figure 1. a) Physical map of Cuf before and after electrodeposition; b) SEM image of Cuf; c) EDS Spectrum of Cuf; d) SEM image of Cuf/Sn; e) EDS spectrum of Cuf/Sn; f) cross section SEM image of Cuf/Sn

To further study the species deposited on Cuf, XRD and FTIR characterization were subjected to both samples. The X-Ray diffractogram of Cuf in Figure 2a reveals that copper foams have face-centered cubic structure (fcc) with high crystallinity regarding the presence of lattice factor (111), (200), and (220) according to JCPDS Card No. 65-9743 (Sen et al., 2014). However, no specific change can be observed on the Cuf/Sn

diffractogram compared to Cuf except the small peak that was observed at 28.96° on the Cuf/Sn that might be attributed to the 110 lattices of SnO_2 (Abdo et al., 2021). This limited result was expected considering the small amount of deposited layer and the majority of oxide present was in the amorphous form. Nevertheless, the FTIR spectrum in Figure 2b clearly shows a difference between Cuf and Cuf/Sn. Owing to the metal character of Cuf, there is no notable infrared absorption can be observed in the Cuf sample. In contrast, the Cuf/Sn shows a clear infrared absorption in the functional group and fingerprint area. The peak at 3446 cm-1 and 1646 cm-1 indicates the presence of O-H stretching and bending vibrations, respectively, owing to the absorbed water and/or oxides terminal bonding (Syauqi et al., 2023). The typical spectrum of Sn oxide bond formation was observed at wavenumber 1401 cm-1, 990 cm-1, and 598 cm-1 which belong to Sn-O-Sn, Sn-OH, and symmetric O-Sn-O bonds, respectively (Akram et al., 2016; Slupska & Ozga, 2014). Furthermore, the Cu2O peak also was observed at 621 cm-1 and 798 cm-1 (Ho et al., 2017) while the CuO peak was observed at 875 cm-1 (Sudha et al., 2021). The results of the characterization using SEM, XRD, and FTIR showed that SnO_2 and the mixture of CuO and Cu_2O were deposited on the Cuf electrode.

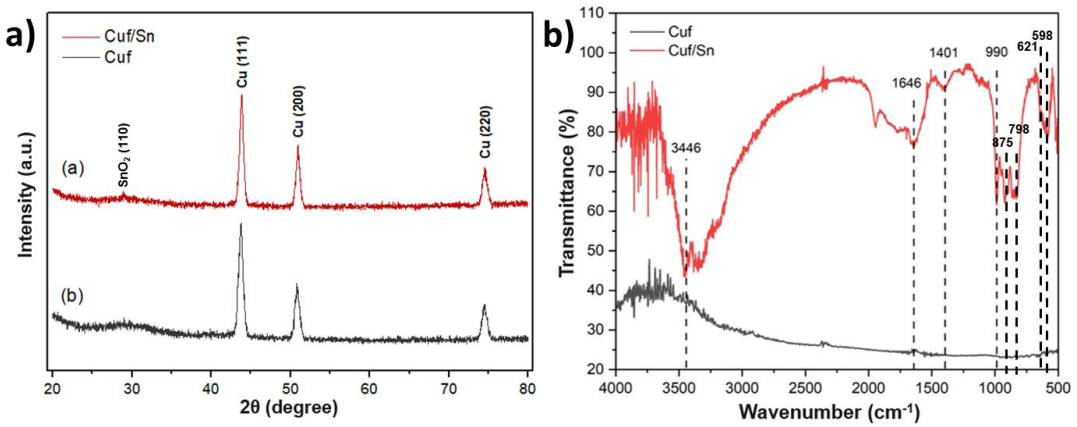

Figure 2. a) XRD pattern of Cuf and Cuf/Sn; b) FTIR spectrum of Cuf and Cuf/Sn

3.2. Electrochemical Properties of Cuf and Cuf/Sn Electrode

The synthesized electrode was then characterized electrochemically by studying the electrochemical active surface area and its activity towards CO_2 reduction. Figure 3 shows the results of the cyclic voltammetry (CV) test for Cuf and Cuf/Sn electrodes carried out at a potential range of 0.5 V to -0.8 V with a scan rate variation of 10 mV/s to 60 mV/s in a 40 mL $K_3Fe(CN)_6$ 1 mM electrolyte in 0.1 M PBS solution pH 7. It is shown in Figure 3a and 3b that both electrodes display a reversible profile with anodic peak potential (Epa) at ~0.2 V and cathodic peak potential (Epc) at ~ –0.3 V owing to the Fe^{2+}/Fe^{3+} redox pair. The difference between Epa and Epc (ΔE) of Cuf/Sn is also higher than Cuf. This phenomenon was attributed to the oxides formed on Cuf after electrodeposition that made the surface of Cuf/Sn less conductive than Cuf. Nevertheless, the anodic peak current (Ipa) and cathodic peak current (Ipc) of each scan rate variation were then recorded and fitted against the square root of the scan rate. Figure 3c and 3d show the results for the Cuf and Cuf/Sn electrodes, respectively. it can be observed that the anodic peak current (Ipa) and cathodic peak current (Ipc) of both electrodes are increased linearly with the increase in scan rate in the range of 10 mV/s to 60 mV/s.

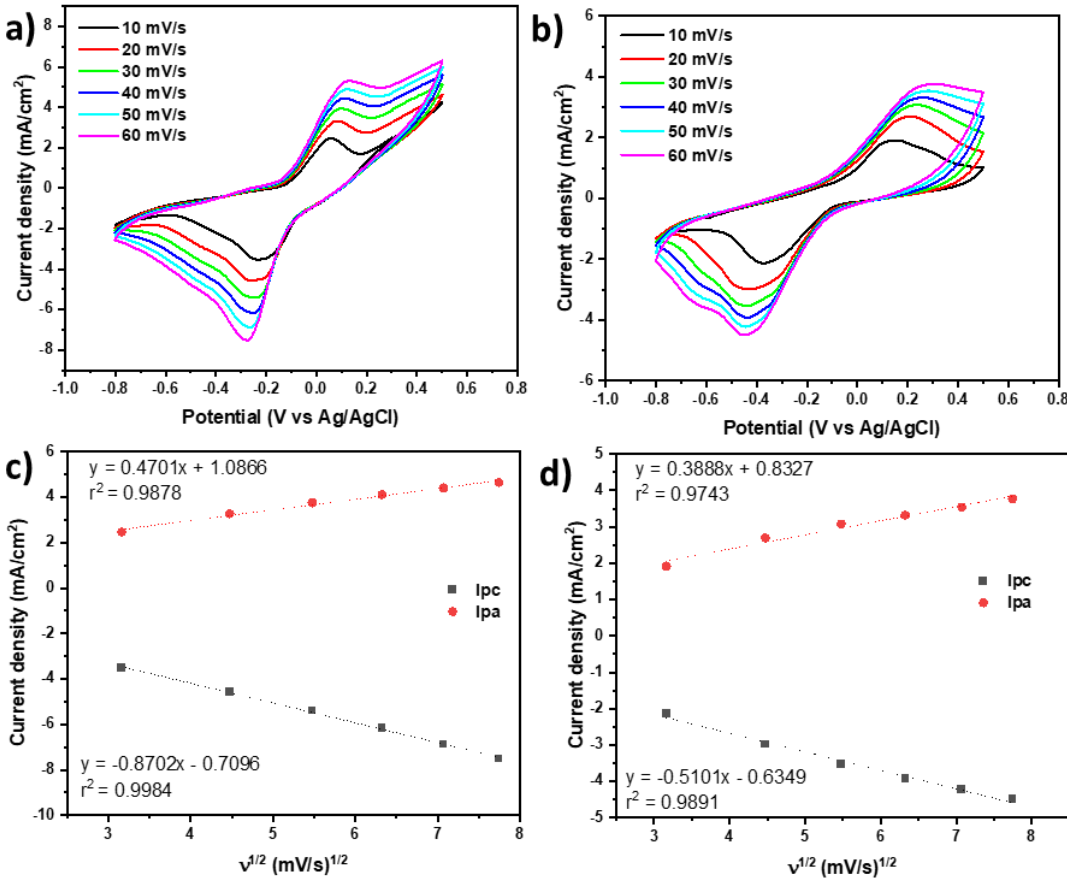

Figure 3. a) Cyclic voltammogram of Cuf, and Cuf/Sn (b) in 1 mM $K_3Fe(CN)_6$ electrolyte in 0.1 M PBS solution with variations of scan rate; c) The linear fit of Ipa and Ipc of Cuf electrode and Cuf/Sn electrode (d) against the square root of scan rate

The relationship between peak current and scan rate can be explained through the Randles-Sevcik equation which is used to calculate the active surface area of the Cuf and Cuf/Sn electrodes. Where Ip = peak current (A), n = electron transferred, D = diffusion coefficient (7.6 x 10^{-6} cm^2/s), v = scan rate (V/s), A = active surface area (cm^2), C = analyte concentration (mol/cm^3), and k = slope on the linear fit.

$$Ip = (2{,}69\ x\ 10^5)\ n^{3/2}\ D^{1/2}\ CAv^{1/2} \qquad (2)$$

$$A = \frac{k}{(2{,}69\ x\ 10^5)\ n^{3/2}\ D^{1/2}\ C} \qquad (3)$$

The calculation result on the active surface area of the non-modified Cu foam (Cuf) and tin-modified Cu foam (Cuf/Sn) electrodes can be seen in Table 1. The presence of the mixture tin-copper oxide layer on the Cuf substrate decreases the electroactive surface area. It caused the lower conductivity of oxide material compared to the Copper. However, this decrease in conductivity is expected to suppress the hydrogen evolution reaction (HER) from water splitting. The presence of Sn species is also expected to boost the performance of forming formic acid as the product of the electroreduction of CO_2 (Proietto et al., 2023).

Table 1. Comparison of the active surface area of Cuf and Cuf/Sn electrodes

Electrode	R^2 Value	Surface Area (cm^2)
Bare Cuf	0.9983	1.1734
Cuf/Sn	0.9891	0.6380

Before testing the electrochemical performance of electrodes to perform a CO_2 reduction reaction (CRR), the saturation condition of the electrolyte was determined. CO_2 gas as a source of CO_2 electroreduction raw material needs to be dissolved into 0.1 M $KHCO_3$. CO_2 gas forms a bicarbonate buffer when aerated into an aqueous electrolyte solution. The aqueous medium acts as a proton donor for CO_2 electroreduction products or intermediates. The equilibrium reaction that occurs is as follows

$$CO_{2\,(g)} \rightleftarrows CO_{2\,(aq)} \quad (4)$$

$$CO_{2\,(aq)} + H_2O_{\,(l)} \rightleftarrows H_2CO_{3\,(aq)} \quad (5)$$

$$H_2CO_{3\,(aq)} \rightleftarrows H^+_{\,(aq)} + HCO_3^-{}_{(aq)} \quad (6)$$

$$HCO_3^-{}_{(aq)} \rightleftarrows H^+_{\,(aq)} + CO_3^{2-}{}_{(aq)} \quad (7)$$

The equilibrium reaction above shows that the amount of CO_2 dissolved in the electrolyte will be proportional to the H^+ ions produced. So that the longer aeration time of CO_2 gas will decrease the pH of the $KHCO_3$ electrolyte solution, while N_2 aeration can remove the dissolved CO_2 and increase the solution pH. It should be noted that in aqueous electrolytes, the CRR competes with hydrogen evolution reaction (HER). Acidic pH conditions not only facilitate protonation but also favor HER than CRR, which can limit Faradaic efficiency for CRR. Thus, electroreduction of CO_2 is generally carried out in a bicarbonate electrolyte, with a near-neutral pH of about 7 and its buffering ability. Figure 4a shows the pH of the solution before and after gas aeration. It can be seen that 15 minutes of N_2 aeration makes the pH of the electrolyte solution increase from pH 8.8 to 9.1 indicating the removal of CO_2 in the solution. After aeration of CO_2 gas for 10 minutes into the electrolyte solution, the pH of the solution decreased to 7.4 which indicates that the aeration of CO_2 gas into the aqueous electrolyte produces H^+ ions which can increase the acidity of the solution which is indicated by a decrease in the pH of the solution. The 20- and 30-min aeration can only decrease the pH up to 7.2.

Next, the CV experiments were conducted using a Cuf working electrode in different aeration conditions to determine the optimum aeration time. Figure 4b shows the increase of current density in reduction and oxidation scan potential for the longer CO_2 aeration time owing to the increased CO_2 concentration. Comparing the 20- and 30-min aeration, the 30-min aeration gave slightly higher current generated than 20-min despite no pH change in the solution. This is because an additional CO_2 gas dissolved or trapped in a solution without forming a bicarbonate ion. Thus, for the reduction application, the 30-min aeration time was used to saturate the electrolyte.

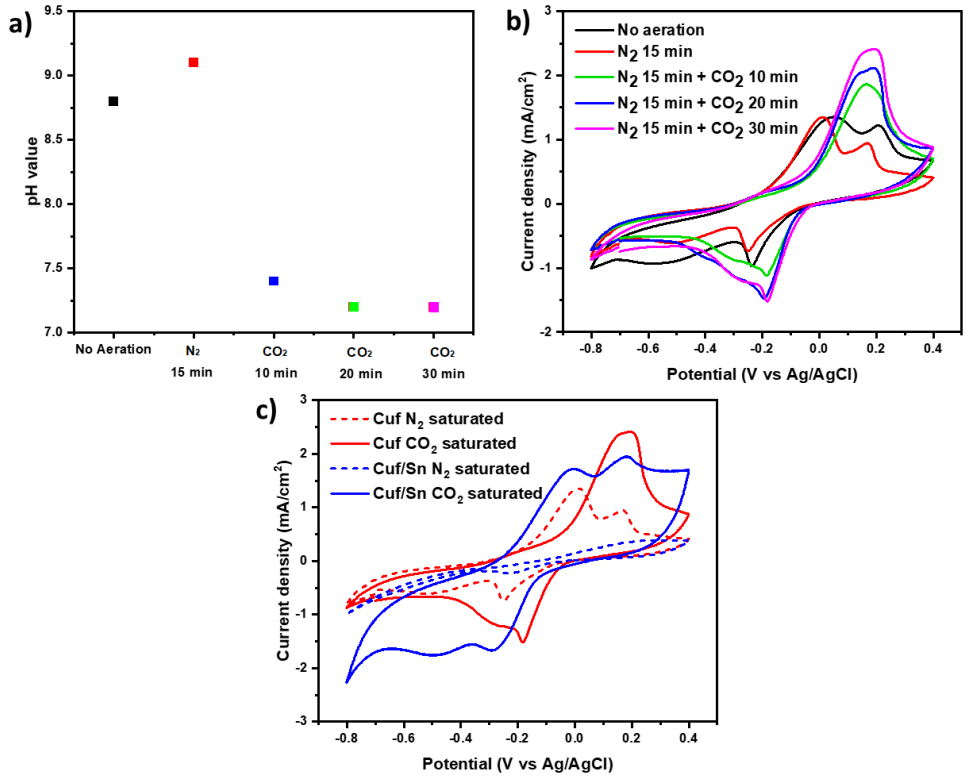

Figure 4. a) pH Measurement of Non-Aerated 0.1 M $KHCO_3$ Electrolyte Solution and after aeration of N_2 and CO_2 gas with Time Variation; b) cathodic linear sweep voltammogram of Cuf/Sn electrode in different electrolyte; c) CV on the Cuf (a) and Cuf/Sn (b) electrode in N_2 and CO_2 saturated 0.1 M $KHCO_3$ at a scan rate of 50 mV/s

In a separate experiment, the CV profile of Cuf and Cuf/Sn electrode in a 0.1 M $KHCO_3$ saturated N_2 and CO_2 gas electrolyte were conducted and compared. As depicted in Figure 4c, it is found that in the negative potential range, in the CO_2 saturated electrolyte, both Cuf and Cuf/Sn give a higher current density compared to the N_2 saturated electrolyte. Moreover, the onset potential for reduction reactions at Cuf shifted to a more positive potential in the CO2-saturated electrolyte, showing the favorability of CO_2 reduction (Yang et al., 2019). While the Cuf/Sn electrode exhibited no significant change in onset potential in both CO_2 and N_2 saturated electrolytes, it generated a higher current in CO_2 saturated electrolyte compared to the Cuf electrode. This suggests a potentially greater activity towards CO_2 reduction reaction (CRR) for the Cuf/Sn electrode, despite its lower electrochemically active surface area. It is also observed that in the N_2 saturated electrolyte where no dissolved CO_2 is present, the Cuf/Sn shows a much lower current density and a more negative onset potential than Cuf, which suggests the lower intrinsic activity of Cuf/Sn towards the HER and higher activity towards CRR to formic acid.

3.3. Performance Analysis of the System for CRR to Formic Acid

The first set of CO_2 reduction experiments was carried out in three different systems namely: Cuf/Sn in batch system, Cuf/Sn in flow system, and Cuf in flow system to directly compare the effect of the flow system and electrodes for the CRR performance to formic acid. The potential applied was –0.5 V in each experiment and a 75 mL/min flow rate was used in the flow system experiment. The result depicted in Figure 5a clearly shows that the flow system increases the produced current density, formic acid yield, and faradaic efficiency (FE) compared to the batch system by 27.46%, 76.23%, and 28.25% respectively. This result is attributed to the enhanced mass transport given by the flow system (Weekes et al., 2018). It has been known that CO_2 reduction in aqueous solution is a multistep process where formic acid is the first stage product along with CO as it only needs 2e transfer to be formed. Thus, the poor mass transport on the electrode surface could lead to further

reaction of formic acid to another reduction product such as formaldehyde, methanol, or methane leading to poor FE towards formic acid (Sun et al., 2017). In the next experiment, Cuf was used as a cathode in the flow cell as a comparison to Cuf/Sn. The result in Figure 5a shows that the Cuf electrode exhibits higher current density than Cuf/Sn owing to the higher conductivity of Cu metal compared to the oxide properties of Cuf/Sn. However, the formic acid yield and FE produced is lower compared to Cuf/Sn. This result proves that the modification of the Cuf electrode by Sn species could enhance the reaction selectivity towards formic acid formation thanks to the synergistic effect of Cu and Sn oxides on the Cuf surface which agrees with the previous report (Zeng et al., 2018; Zoli et al., 2023).

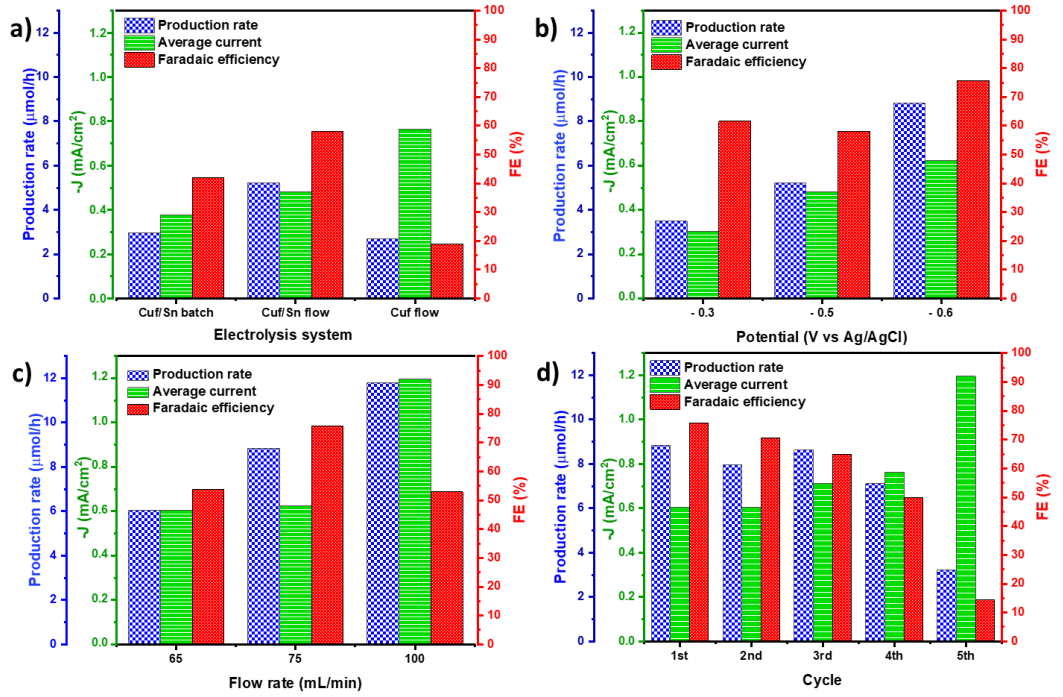

Figure 5. The result of formic acid production rate, average current density, and faradaic efficiency of electrolysis process: a) Different electrolysis systems of Cuf/Sn at –0.5 V applied bias and 75mL/min flow for flow system; b) Variation of applied potential of Cuf/Sn electrode with 75 mL/min flow rate; c) Variation of electrolyte flow rate of Cuf/Sn electrode at –0.6 V applied bias; d) Stability test of Cuf/Sn electrode at –0.6V and 75 mL/min flow rate

To further study and optimize the Cuf/Sn performance for CRR in the flow system, the experiment with bias potential and flow rate variation was conducted. The experiment results of different applied bias potentials (–0.3 V, –0.5 V, and –0,6 V) are shown in Figure 5b. The more negative potential applied here led to the increased formic acid yield and FE. The –0.6 V applied bias with a 75 mL/min flow rate could give a formic acid production rate of 8.84 μmol/h with 75.79% FE. This result can be considered good among reported results on CRR to formic acid system as this reaction uses a relatively positive applied bias compared to other work which usually uses potential more negative than –1.0 V vs Ag/AgCl (Ewis et al., 2023). Thus, the applied bias of –0.6 V was used for the next experiments. In the flow reactor system, the flow rate holds a vital role to enhance the performance. Thus, the attempt to find the optimum flow rate was conducted by varying the flow rate electrolyte to 65mL/min and 100 mL/min. It can be observed from Figure 5c, the increased flow rates lead to the increased current density produced. This is because the increased flow rate, besides enhancing mass transport, could also reduce the overpotential by gradient concentration and improve electrolyte conductivity.

The formic acid production rate of the system with 100mL/min flow rate also reached 11.81 μmol/h, which is the highest in this report. However, the FE calculation showed an optimum value at 75 mL/min with 75.79%, increased from 53.86% at 65

mL/min flow rate and declining to 52.92% at 100 mL/min. This development indicates that at 100 mL/min, the flow rate of electrolyte was exceeding the optimum kinetics rate of CRR to formic acid and instead favoring the hydrogen water splitting reaction or another CRR products such as CO.

Figure 5d shows the repeatability performance on the Cuf/Sn electrode at −0.6 V bias and 75 mL flow rate with one hour reaction time for each cycle. The result shows that the production rate was stable at least until the 4th cycle. Meanwhile, at the 5th cycle, the formic acid yield dropped 63% to 3.22 μmol. It can also be observed that the average current density rose while the FE decayed as the number of experiment cycles increased. This trend might be caused by the gradual change in the Cuf/Sn surface the longer it is used. The change might be because of the exposed Cuf surface. Changes are possible due to several things, including the erosion of the surface oxide layer so that the Cuf surface was exposed and caused the conductivity to increase but the selectivity to decrease. Another possibility is the formation of oxygen vacancy at the electrode as it is used for reduction (L. Li et al., 2020; Liu et al., 2018; Pavithra & Kumar, 2020). Oxygen vacancy can increase the conductivity of the material and increase the adsorption of molecules on the surface. This causes the possibility of formic acid undergoing further electron transfer reactions to become aldehydes, alcohols, or even hydrocarbons (Ji & Luo, 2016).

This work provides better activity towards CRR to formic acid compared to several reports. For example, the Cu-BDD catalyst in a flow cell with 33% FE at – 1.5V vs Ag/AgCl (Zahran Ilyasa et al., 2020) and the Cu/Cu2O catalyst in H-reactor with ~35% FE at −0.6 V vs RHE (C. W. Li & Kanan, 2012). If compared to the report using a similar catalytic system (Cu-Sn oxide), this work provides a comparable performance with the reported H-reactor system. For instance, the work of Fan and Co which used a CuO-SnO_2 (1:1) composite catalyst at −1.00 VSHE, gave ~74% faradaic efficiency (Fan et al., 2018). On the other hand, Yue and co obtained ~65% faradaic efficiency using low crystalline CuO-SnO_2 at −1.00 VSHE (Yue et al., 2023). However, if compared to other Sn-based system catalysts in the flow cell, many have reported the result with > 90% FE and long-term stability as has been reviewed by Ewis and co (Ewis et al., 2023). This comparison provides insight that the room for improvement is still open for our system. Particularly, the optimization of Sn and Cu mol ratio and particle morphology at the catalyst system.

4. Conclusion

In conclusion, the synthesized Cuf/Sn electrodes, achieved through the electrodeposition method, exhibit highly encouraging characteristics for the electrochemical reduction of CO_2 to formic acid. The modified surface of Cuf/Sn was characterized to comprise of Cu_2O, CuO, and SnO_2 mixture layer with an average thickness of 1.65 μm and 0.12% of atomic Sn content confirmed by FTIR, SEM, and XRD characterization. The use of the Cuf/Sn electrode for CO_2 reduction to formic acid produces 75.79% faradaic efficiency, outperforming the Cuf/Sn in the batch system with only 42% faradaic efficiency and Cuf in the flow system with 18.97%. The study highlighted the pivotal role of the synergistic Sn-Cu oxide mixture in suppressing the Hydrogen Evolution Reaction (HER) while promoting CO_2 reduction to formic acid, leading to enhanced performance. The best faradaic efficiency is obtained at 75.79% using Cuf/Sn electrode by 75 mL/min flow rate and −0.6 V (vs. Ag/AgCl) bias with 8.84 mol/h formic acid production rate. By increasing the flow rate to 100 mL/min, the produced formic acid was increased up to 11.81 mmol/h, followed by the decrease of faradaic efficiency to 52.92%. The stability test of the Cuf/Sn electrode reveals consistent performance up to the 4th cycle, with a notable decline at the 5th cycle, likely attributed to the change in the surface properties of the Cuf/Sn electrode.

Author Contribution

Conceptualizing, Data Curation, Visualization, Writing, M.I.S.; Data acquisition, Formal Analysis, Writing – Original Draft Preparation, A.T.C.; Investigation, Validation, Y.M.T.A.P; Formal Analysis, Review & Editing, P.K.J.

Acknowledgement
This work is funded by Hibah PDD DIKTI Republik Indonesia, contract No. NKB-408/UN2.RST/HKP.05.00/2020.

Conflicts of Interest
The authors declare no conflict of interest.

References
Abdo, H. S., Sarkar, A., Gupta, M., Sahoo, S., Mohammed, J. A., Ragab, S. A., & Seikh, A. H. (2021). Low-cost high-performance SnO_2–Cu electrodes for use in direct ethanol fuel cells. *Crystals*, *11*(1), 1–12. https://doi.org/10.3390/cryst11010055

Akram, M., Saleh, A. T., Ibrahim, W. A. W., Awan, A. S., & Hussain, R. (2016). Continuous microwave flow synthesis (CMFS) of nano-sized tin oxide: Effect of precursor concentration. *Ceramics International*, *42*(7), 8613–8619. https://doi.org/10.1016/j.ceramint.2016.02.092

Canadell, J. G., Le Quéré, C., Raupach, M. R., Field, C. B., Buitenhuis, E. T., Ciais, P., Conway, T. J., Gillett, N. P., Houghton, R. A., & Marland, G. (2007). Contributions to accelerating atmospheric CO_2 growth from economic activity, carbon intensity, and efficiency of natural sinks. *Proceedings of the National Academy of Sciences of the United States of America*, *104*(47), 18866–18870. https://doi.org/10.1073/pnas.0702737104

De Gregorio, G. L., Burdyny, T., Loiudice, A., Iyengar, P., Smith, W. A., & Buonsanti, R. (2020). Facet-Dependent Selectivity of Cu Catalysts in Electrochemical CO_2 Reduction at Commercially Viable Current Densities. *ACS Catalysis*, 4854–4862. https://doi.org/10.1021/acscatal.0c00297

El Bahi, B., Galai, M., Cherkaoui, M., & Takenouti, H. (2020). Electrochemical deposition mechanism of copper-zinc-tin alloy and structural characterization. *Surfaces and Interfaces*, *19* (January), 100466. https://doi.org/10.1016/j.surfin.2020.100466

Ewis, D., Arsalan, M., Khaled, M., Pant, D., Ba-Abbad, M. M., Amhamed, A., & El-Naas, M. H. (2023). Electrochemical reduction of CO_2 into formate/formic acid: A review of cell design and operation. *Separation and Purification Technology*, *316* (April), 123811. https://doi.org/10.1016/j.seppur.2023.123811

Fan, M., Ma, C., Lei, T., Jung, J., Guay, D., & Qiao, J. (2018). Aqueous-phase electrochemical reduction of CO_2 based on SnO_2-CuO nanocomposites with improved catalytic activity and selectivity. *Catalysis Today*, *318* (July 2017), 2–9. https://doi.org/10.1016/j.cattod.2017.09.018

Feaster, J. T., Shi, C., Cave, E. R., Hatsukade, T., Abram, D. N., Kuhl, K. P., Hahn, C., Nørskov, J. K., & Jaramillo, T. F. (2017). Understanding Selectivity for the Electrochemical Reduction of Carbon Dioxide to Formic Acid and Carbon Monoxide on Metal Electrodes. *ACS Catalysis*, *7*(7), 4822–4827. https://doi.org/10.1021/acscatal.7b00687

Florides, G. A., & Christodoulides, P. (2009). Global warming and carbon dioxide through sciences. *Environment International*, *35*(2), 390–401. https://doi.org/10.1016/j.envint.2008.07.007

Gonçalves, M. R., Gomes, A., Condeço, J., Fernandes, T. R. C., Pardal, T., Sequeira, C. A. C., & Branco, J. B. (2013). Electrochemical conversion of CO_2 to C_2 hydrocarbons using different ex situ copper electrodeposits. *Electrochimica Acta*, *102*, 388–392. https://doi.org/10.1016/j.electacta.2013.04.015

Ho, W. C. J., Tay, Q., Qi, H., Huang, Z., Li, J., & Chen, Z. (2017). Photocatalytic and adsorption performances of faceted cuprous oxide (Cu_2O) particles for the removal of methyl orange (MO) from aqueous media. *Molecules*, *22*(4). https://doi.org/10.3390/molecules22040677

Ji, Y., & Luo, Y. (2016). New Mechanism for Photocatalytic Reduction of CO_2 on the Anatase TiO_2(101) Surface: The Essential Role of Oxygen Vacancy. *Journal of the American Chemical Society*, *138*(49), 15896–15902. https://doi.org/10.1021/jacs.6b05695

Jiwanti, P. K., Aritonang, R. P., Abdullah, I., Einaga, Y., & Ivandini, T. A. (2019). Copper-nickel-

modified Boron-doped Diamond Electrode for CO_2 Electrochemical Reduction Application: A Preliminary Study. *Makara Journal of Science*, *23*(4), 204–209. https://doi.org/10.7454/mss.v23i4.11512

Jiwanti, P. K., Ichzan, A. M., Dewandaru, R. K. P., Atriardi, S. R., Einaga, Y., & Ivandini, T. A. (2020). Improving the CO_2 electrochemical reduction to formic acid using iridium-oxide-modified boron-doped diamond electrodes. *Diamond and Related Materials*, *106*(April), 107874. https://doi.org/10.1016/j.diamond.2020.107874

Kondratenko, E. V., Mul, G., Baltrusaitis, J., Larrazábal, G. O., & Pérez-Ramírez, J. (2013). Status and perspectives of CO_2 conversion into fuels and chemicals by catalytic, photocatalytic and electrocatalytic processes. *Energy and Environmental Science*, *6*(11), 3112–3135. https://doi.org/10.1039/c3ee41272e

Li, C. W., & Kanan, M. W. (2012). CO_2 Reduction at Low Overpotential on Cu Electrodes Resulting from the Reduction of Thick Cu_2O Films. *Journal of the American Chemical Society*, *134*(17), 7231–7234. https://doi.org/10.1021/ja3010978

Li, L., Zhao, Z.-J., Hu, C., Yang, P., Yuan, X., Wang, Y., Zhang, L., Moskaleva, L., & Gong, J. (2020). Tuning Oxygen Vacancies of Oxides to Promote Electrocatalytic Reduction of Carbon Dioxide. *ACS Energy Letters*, *5*(2), 552–558. https://doi.org/10.1021/acsenergylett.9b02749

Liu, S., Pang, F., Zhang, Q., Guo, R., Wang, Z., Wang, Y., Zhang, W., & Ou, J. (2018). Stable nanoporous Sn/SnO_2 composites for efficient electroreduction of CO_2 to formate over wide potential range. *Applied Materials Today*, *13*, 135–143. https://doi.org/10.1016/j.apmt.2018.08.014

Pavithra, K., & Kumar, S. M. S. (2020). Embedding oxygen vacancies at SnO_2-CNT surfaces: Via a microwave polyol strategy towards effective electrocatalytic reduction of carbon-dioxide to formate. *Catalysis Science and Technology*, *10*(5), 1311–1322. https://doi.org/10.1039/c9cy01960j

Proietto, F., Rinicella, R., Galia, A., & Scialdone, O. (2023). Electrochemical conversion of CO_2 to formic acid using a Sn based cathode: Combined effect of temperature and pressure. *Journal of CO_2 Utilization*, *67* (December 2022), 102338. https://doi.org/10.1016/j.jcou.2022.102338

Saprudin, M. H., Jiwanti, P. K., Saprudin, D., Sanjaya, A. R., Putri, Y. M. T. A., Einaga, Y., & Ivandini, T. A. (2023). Electrochemical reduction of carbon dioxide to acetic acid on a Cu-Au modified boron-doped diamond electrode with a flow-cell system. *RSC Advances*, *13*(32), 22061–22069. https://doi.org/10.1039/d3ra03836j

Sen, S., Liu, D., & Palmore, G. T. R. (2014). Electrochemical reduction of CO_2 at copper nanofoams. *ACS Catalysis*, *4*(9). https://doi.org/10.1021/cs500522g

Slupska, M., & Ozga, P. (2014). Electrodeposition of Sn-Zn-Cu alloys from citrate solutions. *Electrochimica Acta*, *141*, 149–160. https://doi.org/10.1016/j.electacta.2014.07.039

Song, C. (2002). CO_2 Conversion and Utilization: An Overview. *ACS Symposium Series*, *809*, 1–30. https://doi.org/10.1021/bk-2002-0809.ch001

Sudha, V., Murugadoss, G., & Thangamuthu, R. (2021). Structural and morphological tuning of Cu-based metal oxide nanoparticles by a facile chemical method and highly electrochemical sensing of sulphite. *Scientific Reports*, *11*(1), 1–13. https://doi.org/10.1038/s41598-021-82741-z

Sun, Z., Ma, T., Tao, H., Fan, Q., & Han, B. (2017). Fundamentals and Challenges of Electrochemical CO_2 Reduction Using Two-Dimensional Materials. *Chem*, *3*(4), 560–587. https://doi.org/10.1016/j.chempr.2017.09.009

Syauqi, M. I., Khalil, M., Syauqi, M. I., Sanjaya, A. R., & Madiabu, M. J. (2023). *TiO_2 Crystallization at Room Temperature and Preparation of Transparent Carbon Counter Electrode for Low-Cost Dye- Sensitized Solar Cells*. *27*(2). https://doi.org/10.7454/mss.v27i2.1476

Wang, Y., Zhou, J., Lv, W., Fang, H., & Wang, W. (2016). Electrochemical reduction of CO_2 to formate catalyzed by electroplated tin coating on copper foam. *Applied Surface Science*, *362*, 394–398. https://doi.org/10.1016/j.apsusc.2015.11.255

Weekes, D. M., Salvatore, D. A., Reyes, A., Huang, A., & Berlinguette, C. P. (2018). Electrolytic

CO_2 Reduction in a Flow Cell. *Accounts of Chemical Research*, *51*(4), 910–918. https://doi.org/10.1021/acs.accounts.8b00010

Yang, D., Yu, H., He, T., Zuo, S., Liu, X., Yang, H., Ni, B., Li, H., Gu, L., Wang, D., & Wang, X. (2019). Visible-light-switched electron transfer over single porphyrin-metal atom center for highly selective electroreduction of carbon dioxide. *Nature Communications*, *10*(1), 1–10. https://doi.org/10.1038/s41467-019-11817-2

Yang, D., Zhu, Q., & Han, B. (2020). Electroreduction of CO_2 in Ionic Liquid-Based Electrolytes. *Innovation*, *1*(1), 100016. https://doi.org/10.1016/j.xinn.2020.100016

Yue, Y., Zou, X., Shi, Y., Cai, J., Xiang, Y., Li, Z., & Lin, S. (2023). A low crystallinity CuO-SnO_2/C catalyst for efficient electrocatalytic reduction of CO_2. *Journal of Electroanalytical Chemistry*, *928*(December 2022). https://doi.org/10.1016/j.jelechem.2022.117089

Zahran Ilyasa, S., Krisma Jiwanti, P., Khalil, M., Einaga, Y., & Anggraningrum Ivandini, T. (2020). Study of carbon dioxide electrochemical reduction in flow cell system using copper modified boron-doped diamond. *E3S Web of Conferences*, *211*, 1–8. https://doi.org/10.1051/e3sconf/202021103011

Zeng, J., Bejtka, K., Ju, W., Castellino, M., Chiodoni, A., Sacco, A., Farkhondehfal, M. A., Hernández, S., Rentsch, D., Battaglia, C., & Pirri, C. F. (2018). Advanced Cu-Sn foam for selectively converting CO_2 to CO in aqueous solution. *Applied Catalysis B: Environmental*, *236*(May), 475–482. https://doi.org/10.1016/j.apcatb.2018.05.056

Zoli, M., Roldán, D., Guzmán, H., Castellino, M., Chiodoni, A., Bejtka, K., Russo, N., & Hernández, S. (2023). Facile and scalable synthesis of Cu_2O-SnO_2 catalyst for the photoelectrochemical CO_2 conversion. *Catalysis Today*, *413–415*, 113985. https://doi.org/10.1016/j.cattod.2022.12.016